A shielded hot-wire probe to detect flow reversals with one-dimensional pulsating flow

Benjamin, S.F., Liu, Z. and Roberts, C.A.

Original citation & hyperlink:
Benjamin, S.F. , Liu, Z. and Roberts, C.A. (2004) A shielded hot-wire probe to detect flow reversals with one-dimensional pulsating flow. Proceedings of the Institution of Mechanical Engineers, Part C: Journal of Mechanical Engineering Science, volume 218 (7): 797-801.
http://dx.doi.org/10.1243/0954406041319572

Flow measurements across an automotive catalyst monolith situated downstream of a planar wide-angled diffuser.

S. S. Quadri, S. F. Benjamin* and C. A. Roberts

Automotive Engineering Applied Research Group, Faculty of Engineering and Computing, Coventry University, Coventry CV1 5FB U.K.

**Corresponding author. Tel.: +44 (0) 2476 888362*
E-mail address: s.benjamin@coventry.ac.uk
Postal address: Maurice Foss Building, Faculty of Engineering and Computing, Coventry University, Priory St, Coventry CV1 5FB, UK

Abstract

Flow measurements are presented across an automotive catalyst monolith situated downstream of a planar wide-angled diffuser. Particle Image Velocimetry (PIV) measurements were obtained in the diffuser and the flow distribution within the monolith was obtained from hot wire anemometry (HWA) at the monolith exit. Flow separation at the diffuser inlet resulted in the formation of a jet which traversed the diffuser before spreading just prior to entering the monolith. The jet featured a potential core and saddle-type velocity profiles. A free shear layer separated the jet core from two large recirculation regions which developed in the diffuser narrowing the potential core. The flow field in the main body of the diffuser was observed to be independent of Re in contrast to that within the monolith. Increasing monolith length gave greater flow uniformity in the monolith as a consequence of jet spreading. Comparing the axial velocity flow profiles ~ 3 mm upstream of the monolith to that downstream showed that significant flow redistribution occurred as the flow entered the monolith resulting in more flow entering peripheral channels. It is inferred that pressure loss arising from oblique entry into monolith channels significantly affects the flow distribution within the monolith.

Keywords: PIV; Automotive catalyst; Monolith, Planar wide-angled diffuser; Oblique entry; Pressure loss; Flow maldistribution

1. INTRODUCTION

Automotive catalytic converters are extensively used to reduce vehicle exhaust emissions to enable compliance with regulations. A typical converter consists of a monolith encased in a metal casing. The monolith can be made of ceramic, usually cordierite, or metal and normally comprises of a large number of parallel channels of small hydraulic diameter ~1mm through which the exhaust gas flows. This provides the high surface area required for maximum conversion efficiency. The channels are coated with a thin porous washcoat embedded in which are the precious metal catalysts which promote reactions. One important factor that determines conversion efficiency is the flow distribution or residence time in the monolith which should be uniform for optimum performance. In practice converters have to be fitted in a confined space within the exhaust system whilst ensuring sufficient volume is maintained for adequate conversion efficiency. This necessitates a large expansion to connect the exhaust pipe to the front face of the converter, which results in flow separation at the diffuser inlet and non uniform flow entering the monolith. Figure 1 shows a typical exhaust catalyst assembly featuring two monoliths located downstream of a wide angled diffuser along with a representation of the flow field within the diffuser. As a consequence of non uniform flow entering the monolith large sections of the catalyst are poorly utilised. This has a detrimental effect on conversion efficiency, catalyst durability and system pressure loss. Increasingly, flow maldistribution across the monolith is used to assess the acceptability of design concepts and computational fluid dynamics (CFD) is often employed to provide this information.

Factors influencing the monolith flow distribution are the diffuser geometry, the monolith resistance and the flow conditions at inlet to the diffuser. The majority of monoliths comprise straight parallel channels and the flow distribution within the monolith can be inferred from measurements obtained at the monolith exit where the flow emerges axially. Hence the effect of various designs can be assessed. In order to assess their accuracy, CFD predictions are often compared with measurements obtained at the monolith exit **[1, 2]**. When modelling monolith resistance it is usually assumed that the pressure loss within channels can be estimated using either the Hagen-Poiseuille **[3]** or Shah **[4]** expressions as the flow is normally laminar. Studies by the present authors **[5, 6]** have shown that simulations need also to account for monolith losses associated with oblique flow impingement at the channel entrance.

Figure 1 illustrates that away from the centre line the flow approaches the monolith obliquely leading to flow separation at the channel entrance and a significant additional pressure loss. Benjamin et al **[5]**, using an expression for oblique entry losses developed by Küchemann and Weber **[7]** for heat exchangers, obtained improved predictions for axisymmetric systems. Recently these losses have been measured by Persoons et al **[8]** and the present authors **[9]**.

There have been few studies where measurements both within the upstream diffuser and downstream of the monolith have been reported. The flow field in the former is difficult to measure as the geometry is often complex and the flow three dimensional. Early studies by Wendland et al **[10]** employed flow visualisation. Kim et al **[11]** measured the axial velocity 1 mm upstream of the leading face of a monolith using Laser Doppler Anemometry for an axisymmetric assembly at two Reynolds numbers (Re). They showed that the flow profiles were less uniform at the higher Re. Interestingly they obtained very good agreement with CFD predictions. The monolith was modelled assuming a resistance based on the Darcy equation with a correction for an entrance effect for developing flow. Unfortunately they did not measure velocity profiles at the outlet of the monolith. More recently studies have been performed using PIV. Shuai et al **[12]** used PIV to measure the flow field in the diffuser of axisymmetric systems. They examined the effect of diffuser and monolith designs and showed comparisons with CFD predictions. In particular they show profiles of axial and radial velocities at distances of 1.8 and 5.5 mm from the inlet face of the monolith. The flow is observed to spread significantly over this distance. Comparisons with predictions show discrepancies in the radial component attributed in part to inaccuracies in the modelling of the monolith. Ilgner et al **[13]** applied PIV to measure the flow distribution in a diffuser upstream of a monolith used as an autothermal gasoline reformer. Due to difficulties with optical access significant image distortion was evident with light-scattering problems near walls. This restricted the field of view where reliable data could be obtained.

The study reported here presents measurements made both upstream and downstream of monoliths using a planar diffuser. Although the geometry is relatively simple it captures the primary flow features of production-type configurations i.e. separated flow in diffusers placed upstream of monoliths. The planar configuration permits full field mapping thus providing a useful data base for comparison with

CFD at a later date. Assessing CFD performance for this case is considered a necessary starting point prior to evaluation of more complex systems.

2. TWO-DIMENSIONAL FLOW RIG

Figure 2 shows a schematic of the 2-D planar isothermal flow rig; further detail is given in **[14]**. A planar diffuser was chosen so that PIV measurements could be taken with minimal optical distortion with two sides of the diffuser made of plane high transmission crown glass. The rig was designed to provide uniform velocity at inlet to the diffuser in order to give well defined boundary conditions for CFD modelling. To achieve this a plenum chamber, of cross section 220 x 220mm was connected to a contracting nozzle with rectangular outlet 55 x 220mm. A flow straightener was placed close to the exit of the plenum chamber (inlet to the nozzle) in order to reduce non-uniformities in the flow profile. The diffuser had a total included angle of 60 degrees, length 108.2 mm and an area ratio of 3.27. Cordierite monoliths with lengths of either 27 or 100 mm were placed downstream of the diffuser. An outlet sleeve of length 30 mm was positioned downstream of the monolith in order to obtain flow profiles at monolith exit. The monolith was unwashcoated with square channels of hydraulic diameter 1.12mm, a nominal cell density of 62 cells/cm^2, and a porosity of 0.77. Velocity profiles at the exit of nozzle and monolith were obtained using a TSI IFA 300 constant temperature hot-wire anemometry system (HWA). The probes used were 5μm platinum plated tungsten wires (Dantec 55 P11) and were calibrated using a fully automatic TSI 1129 calibration rig. A sampling size of 2048 points per channel and a sampling rate of 2000 Hz was used and velocity recorded at spacings of 2.5 mm. Velocity profiles at nozzle exit were obtained with the diffuser, monolith and outlet sleeve disconnected. Figure 3 shows that profiles at the nozzle were reasonably flat thus providing a good approximation to planar conditions with only a slight asymmetry evident along the x-axis.

The PIV system was supplied by TSI and consisted of a 532 nm Nd:YAG laser with pulse duration of 5ns, pulse energy of 120 mJ and a repetition rate of 15 Hz. The laser was mounted on a bench and aligned perpendicular to the rig and the camera. A spherical lens of 1000 mm focal length was used in combination with a cylindrical lens to obtain a light sheet. The rig was placed at approximately 750 mm from the laser resulting in a light sheet thickness of 1 mm across the field of view. A

POWERVIEW 4M camera from TSI was mounted on a custom designed traverse. The camera has a resolution of 2048 × 2048 pixels with pixel size of 7.4 × 7.4 μm. Seeding particles were injected into the flow from a TSI six-jet atomiser. Olive oil was used for seeding and the atomiser pressure was set to 25 psi, the particle diameter being about 1-2 μm **[15]**. To achieve uniform seeding a manifold was designed so the seeding entered the flow through the four sides of the plenum chamber. To observe the complete flow field in the diffuser required a field of view of 180 x 180 mm. Westerweel **[16]** suggested a particle image diameter of 2 pixels for digital PIV analysis. Initial tests were performed by using an f number in the range of 4-8 and the results showed that a particle image diameter above 1 pixel resulted in good quality vectors. This was a compromise between the requirement for a large field of view and the optimum particle image diameter. Three different fields of view were investigated, namely full-field (180 × 90 mm), half-field (90 × 60 mm) and near-wall field (45 × 40 mm), as shown in figure 4.

PIV experiments were conducted for two different lengths of monolith, 100 and 27 mm, and at five different flow rates corresponding to Re between 27500 and 46500 based on the equivalent hydraulic diameter of the rectangular nozzle. Due to reflection from the surface, close to the diffuser-monolith interface, accurate measurements of vectors very close to the interface (approximately 2 mm) were not possible for all three fields of view. Hence PIV results exclude the region 2 mm upstream of the interface. PIV images were processed using INSIGHT-3G software and post-processed using Tecplot 10. Around 95 % of data obtained was from first-choice vectors and the median and the mean value of surrounding vectors were used to remove spurious data. The error in velocity measurements was around 4-5 %. Experimentation showed that a sample size of 50 images was adequate. The recursive Nyquist grid method was used to process the data with an initial grid size of 64 × 64 pixels and a final grid of 32 × 32 pixels.

3. RESULTS AND DISCUSSION

Figures 5 a & b shows the full field-of-view vector field and contour plot for the velocity magnitude and figures 5c & d contour plots for axial and lateral velocity at Re:41800 for the 27mm monolith.

Flow separation at inlet to the diffuser results in the formation of a jet which traverses the diffuser before rapidly spreading prior to entering the monolith. Part of the flow enters the monolith, the rest returning to feed two large recirculating vortices which occupy the diffuser volume. A free shear layer separates the jet core from these vortices. There is a slight asymmetry in the flow presumably reflecting that of the inlet profile.

Figure 6 shows axial velocity profiles non-dimensionalised by the average velocity at diffuser inlet. Profiles are shown at different locations downstream of the diffuser for three flow rates obtained from the half-field of view measurements. On entering the diffuser profiles resemble those of a plane free jet with a potential core. Non-dimensional velocities greater than 1 are observed at the centre of the jet near the inlet as the two large recirculating vortices formed in the diffuser cause narrowing of the potential core. Around 40 mm from the diffuser-monolith interface saddle-shape profiles develop. Similar saddle-shape features have also been found in rectangular free jets, **[17, 18]**, their origin being the subject of much speculation. Here the situation is somewhat different, however, as the jet is bounded and will be clearly influenced by the recirculating vortices in the diffuser. In this case it would appear that these vortices "feed" the jet resulting in secondary velocity peaks at its periphery. The saddle-shapes develop and become more prominent at around 35 mm from the diffuser-monolith interface. The profiles lose their saddle-shape at about 15 mm from inlet of the monolith as the flow spreads. The flow field is independent of Re in contrast to the flow maldistribution within the monolith, discussed below.

Figure 7 compares 27 mm and 100 mm monoliths. The flow field is largely unaffected by the increased monolith resistance up to about 68 mm from the diffuser-monolith interface. Closer to the interface the higher resistance of the 100 mm monolith results in a flattening of the axial velocity profile.

Near the monolith the jet spreads due to the lateral pressure gradient that develops as higher velocity fluid at the jet centre-line encounters high monolith resistance on entering the central channels. This results in oblique entry into channels away from the jet centre-line as can be seen in figure 8 where at distances beyond 60mm from the centre-line the flow approaches the monolith at very high incidence, ~ 80 degrees and above. This further restricts flow into the monolith at these locations and forces the

flow towards the periphery. Figure 8 shows flow stagnating at the diffuser wall approximately 7mm from the inlet of the monolith about 80 mm from the centre-line. Below the stagnation point the flow is observed to be turning into the outermost channels.

Hot wire velocity measurements were made 30mm downstream of the monolith. At this distance individual jets from neighbouring channels have mixed sufficiently to provide smooth profiles, **[2]**. Figure 9 shows the non-dimensionalised axial velocities profiles for monolith lengths 27 mm and 100 mm at two flow rates. For both monoliths flow maldistribution increases with Re, especially for the shorter monolith. Secondary velocity peaks are observed near the walls of the diffuser. Similar peaks have been observed for axisymmetric systems, **[2]**. Figure 10 compares the downstream HWA profile with the PIV profile obtained at the closest practical distance from the inlet of the 27mm monolith. Clearly the flow redistributes significantly just upstream of the monolith with outward flow forcing fluid into the outermost channels resulting in the secondary peaks in figure 9. This observation is consistent with the findings of Persoons et al. **[19]** who measured velocities up to 0.3mm from the inlet of a monolith presented with swirling flow. They showed a significant swirl component even at such close proximity to the monolith. The degree of redistribution will clearly depend on the oblique entry losses as the flow enters the monolith as these will have a significant effect on the lateral pressure gradient at the inlet of the monolith. These losses have recently been measured by the present authors, **[9]**. Experiments were performed on a specially designed flow rig using monoliths of different lengths (17-100mm) over a range of Reynolds number and angles of incidence (0-75 degrees). Oblique entry pressure losses were found to be a function of Reynolds number and angle of incidence. At high angle of incidence these losses were much greater than those associated with wall shear stresses within the monolith channels. CFD predictions were also performed for axisymmetric catalyst assemblies and compared to HWA measurements obtained downstream of the monolith in a previous study **[5]**. When oblique entry losses were incorporated the predicted flow distribution within the monolith provided much better agreement with experimental data with the assumption that such losses were constant above an angle of incidence of 81 degrees. For the axisymmetric study **[5]** measurements within the diffuser were not made. The present study, along with the results from Quadri et al. **[9]** will provide a useful data base for assessing the performance of CFD in predicting the flow distribution both within the planar diffuser and the monolith. This is a subject of ongoing research.

4. CONCLUSIONS

The flow field has been studied for the case of a 2D planar wide angled diffuser placed upstream of automotive catalyst monoliths. PIV measurements were obtained within the diffuser and the flow distribution within the monolith was obtained from HWA measurements near the monolith exit. The main conclusions from this study are:

- Flow separation at the diffuser inlet resulted in the formation of a jet which traversed the diffuser before spreading prior to entering the monolith. The jet featured a potential core and saddle-type velocity profiles. A free shear layer separated the jet core from two large recirculation regions which developed in the diffuser narrowing the potential core near the inlet.
- The flow field in the diffuser was observed to be independent of Re in contrast to flow maldistribution in the monolith which increased with Re.
- Increasing monolith length gave greater flow uniformity in the monolith as a consequence of jet spreading.
- Lateral profiles of the axial velocity ~3mm upstream of the monolith were significantly different to those observed downstream demonstrating that the flow within the monolith is highly dependent on its behaviour as it enters the monolith channels.
- It is inferred that oblique entry losses at the channel entrance significantly affect the flow distribution within the monolith.
- The results of this study and those of Quadri et al **[9]** will provide a useful data base for assessing the performance of CFD in predicting the flow distribution both within the diffuser and monolith.

REFERENCES

1. **Weltens, H., Bressler, H., Terres, F., Neumaier, H.,** and **Rammoser, D.,** Optimisation of catalytic converter gas flow distribution by CFD prediction SAE Paper 930780, 1993. Also published in SP-957 pp 131-151 SAE International, Warrendale, PA , USA.

2. **Benjamin, S. F., Clarkson, R. J., Haimad, N.** and **Girgis, N. S.** An experimental and predictive study of flow in axisymmetric automotive exhaust catalyst systems. *SAE Trans., J. Fuels and Lubricants*, 1996 **105**, Sec. 4, 1008-1019

3. **Shah, R. K.** and **London, A. L.** *Laminar flow forced convection in ducts,* 1978 (Academic Press).

4. **Shah, R. K.** A correlation for laminar hydrodynamic entry length solutions for circular and noncircular ducts. *Transactions of the ASME, Journal of Fluids Engineering*, 1978, **100**, 177-179.

5. **Benjamin, S. F., Haimad, N., Roberts, C. A.,** and **Wollin, J.** Modelling the flow distribution through automotive catalytic converters. *Proc. Inst. Mech. Engrs, Part C: J. Mechanical Engineering Science*, 2001, **215** (C4), 379-383.

6. **Benjamin, S. F., Zhao, H.** and **Arias-Garcia, A.** Predicting the flow field inside a close-coupled catalyst-the effect of entrance losses. *Proc. Inst. Mech. Engrs, Part C: J. Mechanical Engineering Science*, 2002, **217** (C4), 283-288.

7. **Küchemann, D.** and **Weber, J**. *Aerodynamics of propulsion,* 1953 (McGraw-Hill, New York).

8. **Persoons, T., Vanierschot, M.** and **Van den Bulck, E.** Oblique inlet pressure loss for swirling flow entering a catalyst substrate, *Exp. Therm. Fluid Sci*., 2008, **32**, 1223-1231.

9. **Quadri, S. S., Benjamin, S. F.** and **Roberts, C. A.** Experimental investigation of oblique entry pressure losses in automotive catalytic converters, *Proc. Inst. Mech. Engrs , Part C:J. Mechanical Engineering Science*, 2009, (in press) DOI: 0.1243/09544062JMES1565.

10. **Wendland, D. W.** and **Matthes, W. R.** Visualisation of Automotive Catalytic Converter Internal Flow, *SAE Trans., J. Fuels and Lubricants*, 1986, **95**.

11. **Kim, J. Y., Lai, M.-C., Li, P.** and **Chui, G. K.** Flow distribution and pressure drop in diffuser-monolith flows, *Transactions of the ASME, Journal of Fluids Engineering*, 1995, **117**, 362-368.

12. **Shuai, S.-J., Wang, J.-X., Dong, Q.-L.** and **Zhuang, R.-J.** PIV measurement and numerical simulation of flows in automotive catalytic converters, SAE Paper 2001-01-3494, 2001. Also published in SP-1638 SAE International, Warrendale, PA, USA.

13. **Ilgner, F., Nau, M., Harndorf, H., Benninger, K., Schiessl, R., Maas, U.** and **Dreizler, A.** Analysis of flow patterns inside an autothermal gasoline reformer, SAE Paper 2001-01-1917, 2001.

14. **Quadri, S. S.** The effect of oblique entry flow in automotive catalytic converters. Ph.D. thesis, Coventry University, U.K, 2008.

15. **Melling, A.** Tracer particles and seeding for particle image velocimetry, *Meas. Sci. Technology*, 1997, **8,** 1406-1416.

16. **Westerweel J.** Digital particle image velocimtery, theory and application, PhD thesis, Technische Universiteit Delft, Netherlands, 1993.

17. **Marsters, G. F.** Spanwise velocity distributions in jets from rectangular slots, *AIAA Journal*, 1981, **19** (2), 148-152.

18. **Quinn W. R.** Development of a large-aspect-ratio rectangular turbulent free jet, *AIAA Journal*, 1994, **32** (3), 547-554.

19. **Persoons, T. Vanierschot, M.** and **Van den Bulck, E.** Stereoscopic PIV measurements of swirling flow entering a catalyst substrate, *Exp. Therm. Fluid Sci*., 2008, **32**, 1590-1596.

Figure captions

Fig. 1 Schematic diagram showing catalyst configuration comprising of two monoliths in an exhaust system, catalyst channels and flow separation in a diffuser **[8].**

Fig. 2 2-D isothermal flow rig.

Fig. 3 Velocity profiles at the plane of nozzle exit (x and z axes).

Fig. 4 Field of view regions in the diffuser for PIV measurements. AB corresponds to the diffuser-monolith interface. O corresponds to the centre of diffuser-monolith interface.

Fig. 5 PIV plots for Re; 41800, 27 mm monolith (a) velocity vectors, (b) velocity magnitude , (c) axial velocity and (d) lateral velocity, units (m/s).

Fig. 6 Profiles of non-dimensional axial velocity in the diffuser for the 27 mm monolith at various Re: Y is distance from the inlet of the monolith; velocity normalised by inlet velocity.

Fig. 7 Profiles of axial velocity in the diffuser for 27 mm and 100 mm monolith, Re: 46500 (legends in figures show the axial distance from the diffuser-monolith interface).

Fig. 8 Near-wall field of view vector plot; Re: 41800, 27 mm monolith.

Fig. 9 Non-dimensional axial flow distribution 30 mm from the exit; 27 mm and 100 mm monoliths; velocity normalised by mean velocity at exit of monolith.

Fig. 10 Axial velocity profiles 3.28 mm upstream (PIV) and 30 mm downstream (HWA); Re 41800, 27 mm monolith.

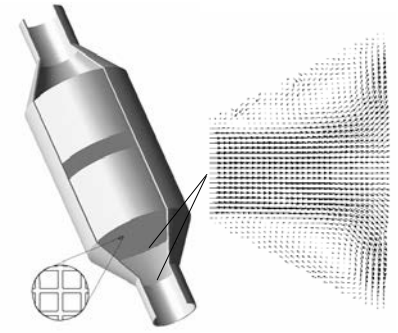

Fig. 1 Schematic diagram showing catalyst configuration comprising of two monoliths in an exhaust system, catalyst channels and flow separation in a diffuser **[9].**

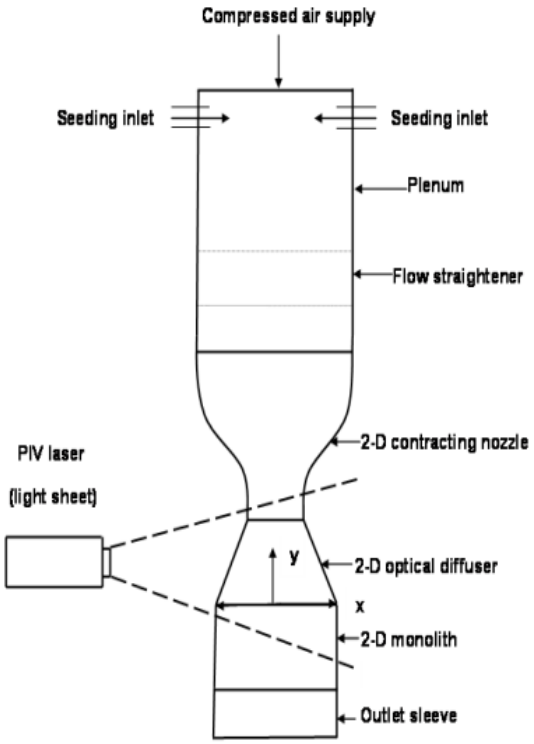

Fig. 2 2-D isothermal flow rig.

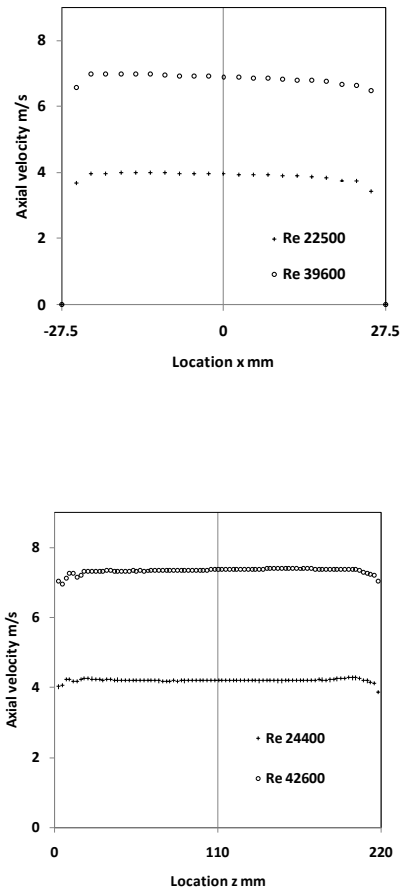

Fig. 3 Velocity profiles at the plane of nozzle exit (x and z axes).

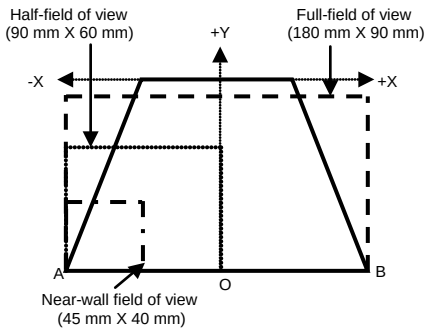

Fig. 4 Field of view regions in the diffuser for PIV measurements. AB corresponds to the diffuser-monolith interface. O corresponds to the centre of diffuser-monolith interface.

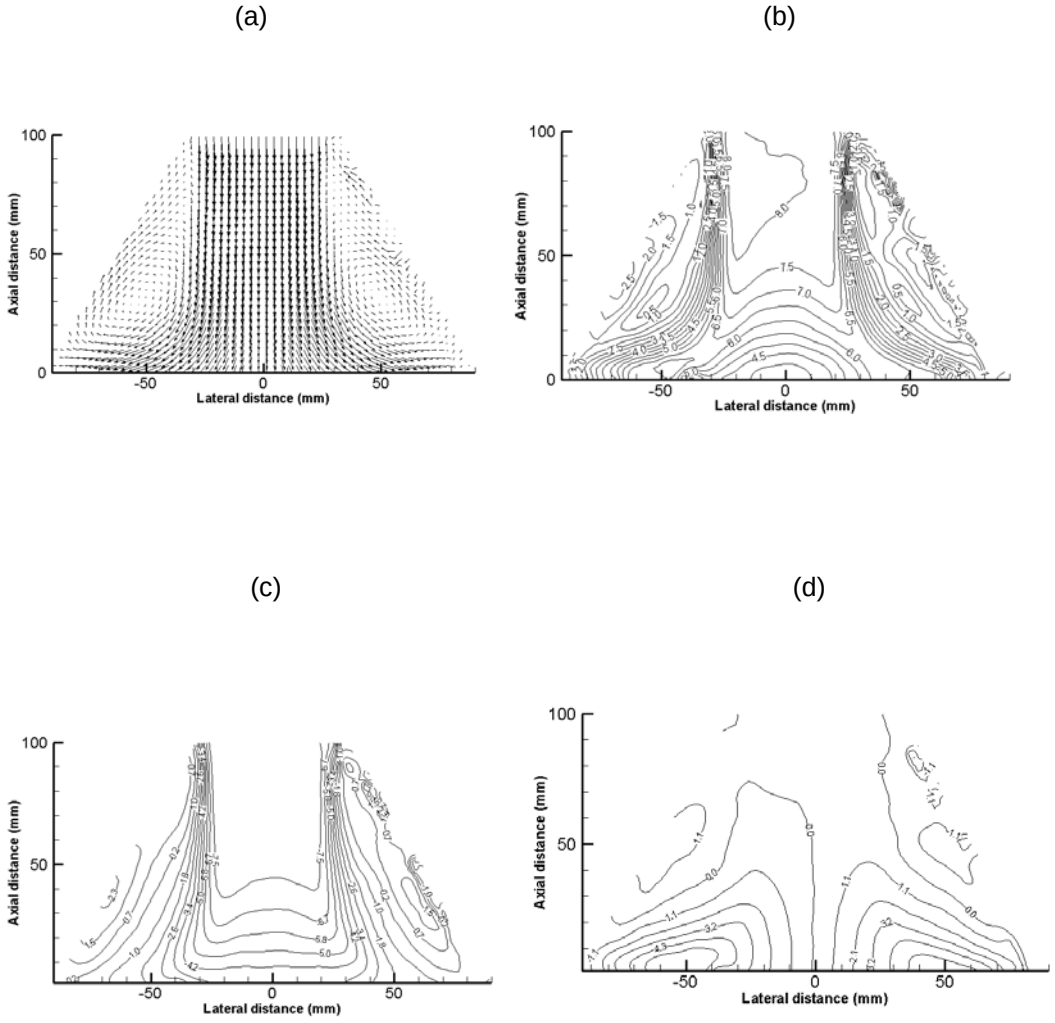

Fig. 5 PIV plots for Re; 41800, 27 mm monolith (a) velocity vectors, (b) velocity magnitude , (c) axial velocity and (d) lateral velocity, units (m/s).

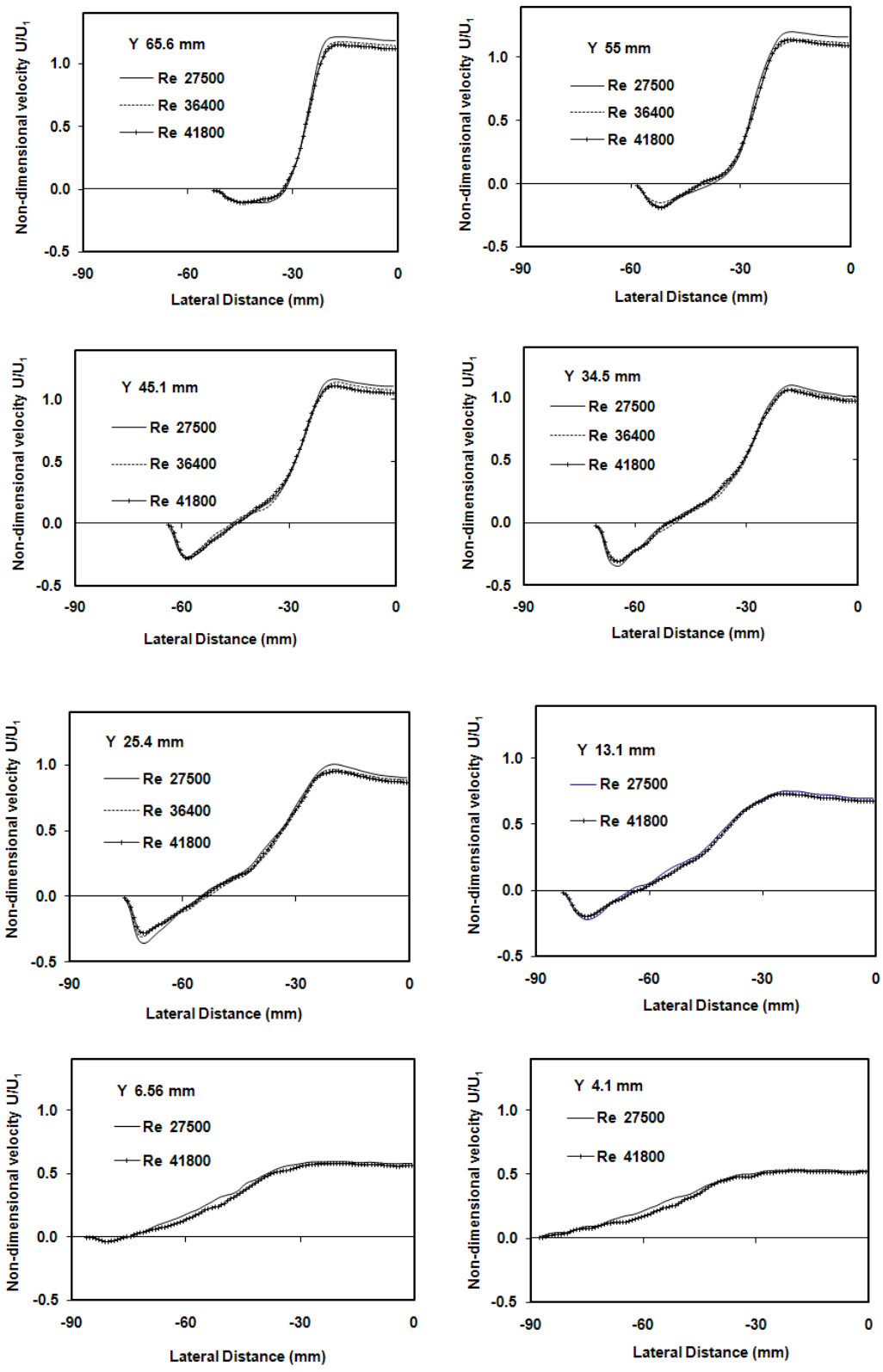

Fig. 6 Profiles of non-dimensional axial velocity in the diffuser for the 27 mm monolith at various Re: Y is distance from the inlet of the monolith; velocity normalised by inlet velocity.

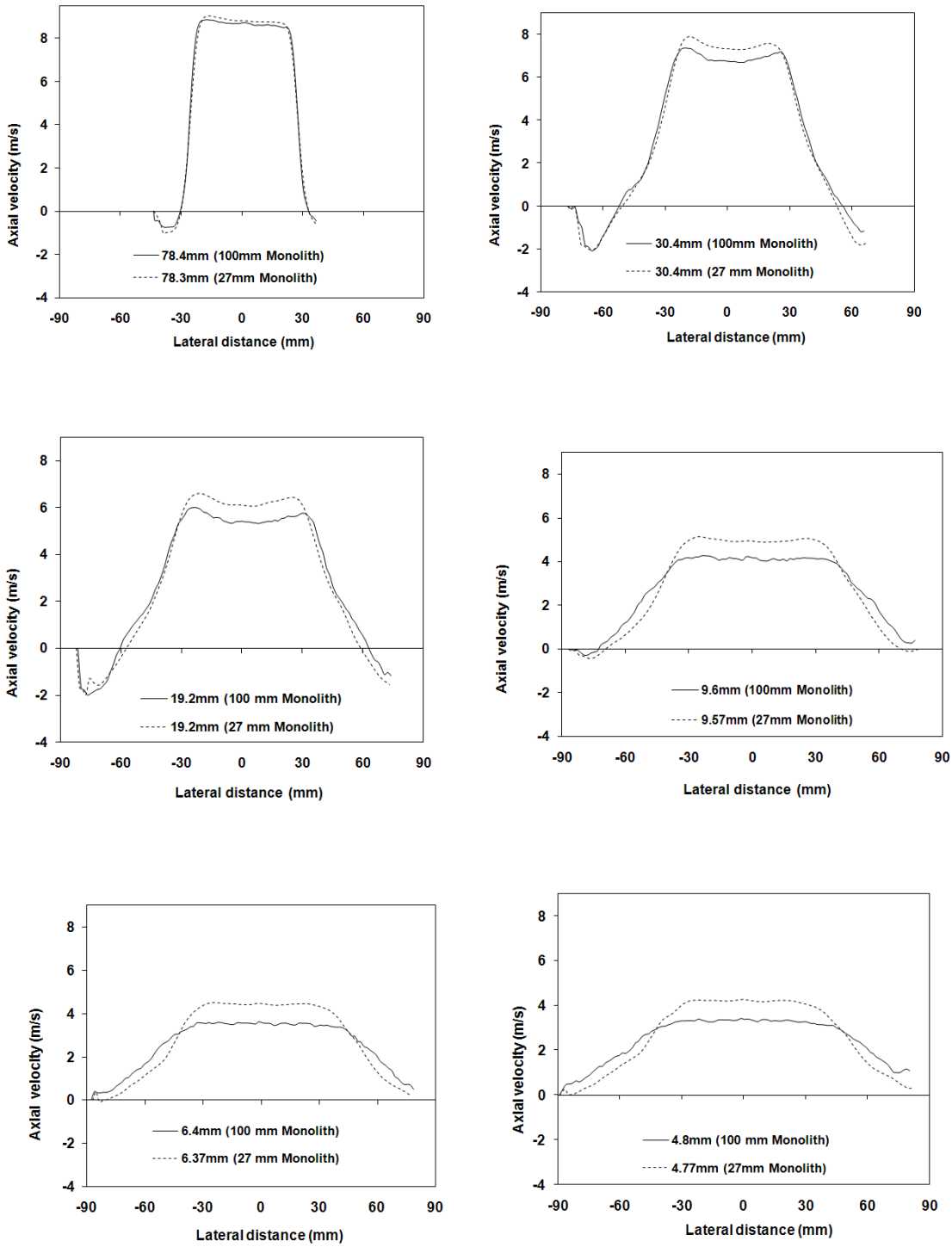

Fig. 7 Profiles of axial velocity in the diffuser for 27 mm and 100 mm monolith, Re: 46500 (legends in figures show the axial distance from the diffuser-monolith interface).

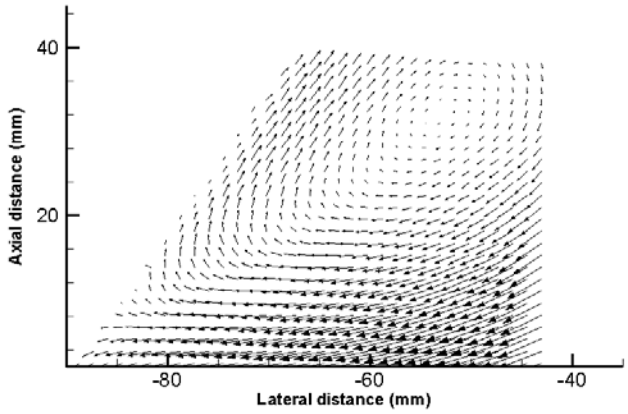

Fig. 8 Near-wall field of view vector plot; Re: 41800, 27 mm monolith.

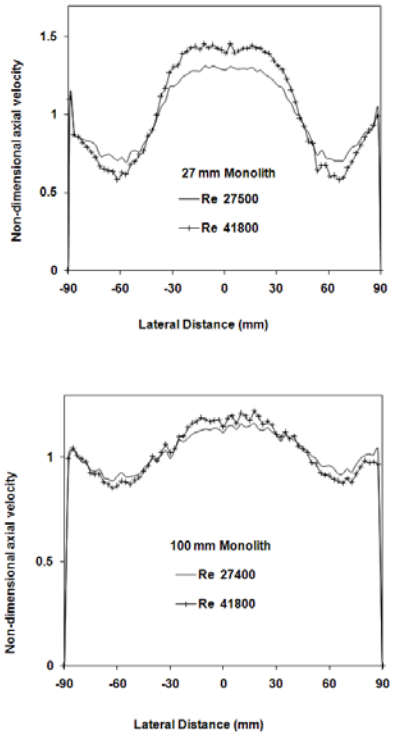

Fig. 9 Non-dimensional axial flow distribution 30 mm from the exit; 27 mm and 100 mm monoliths; velocity normalised by mean velocity at exit of monolith.

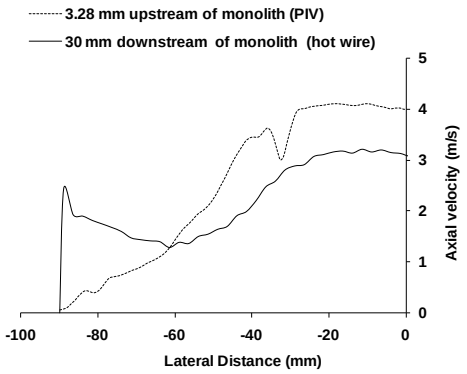

Fig. 10 Axial velocity profiles 3.28 mm upstream (PIV) and 30 mm downstream (HWA); Re 41800, 27 mm monolith.